A Model for the Thermally Assisted Diffusion of Hydrogen in Zirconium Alloys

Research · November 2015

DOI: 10.13140/RG.2.1.1260.7443

1 author:

Manuel Quecedo
ENUSA Industrias Avanzadas
31 PUBLICATIONS **606** CITATIONS

SEE PROFILE

A Model for the Thermally Assisted Diffusion of Hydrogen in Zirconium Alloys and its FEM Solution

M. Quecedo* and Cristina Muñoz-Reja
ENUSA Industrias Avanzadas
Santiago Rusiñol 12, 28040 Madrid, Spain
Corresponding Author
e-mail: mqg@enusa.es
Phone number: +34 606 769 716

February 23, 2015

Abstract

Being the smallest atom, hydrogen can diffuse easily through metals, and their alloys, under concentration and thermal gradients precipitating and affecting their properties. Therefore, much effort has been devoted to understand and to model the thermally assisted diffusion of hydrogen through metals.

This paper presents the derivation of the model equations, stressing that they can be cast as advection-diffusion with sources. From this field, the authors propose to use a well proved method, an splitting procedure based on the aplication of the Two Step Taylor-Galerkin method and the integration of the ODE corresponding to the sources, to solve the model equations.

Due to its effect in the performance of the alloys used by the nuclear industry, hydrogen migration and precipitation in zirconium dilute alloys has been already characterized. Using the available material properties, the numerical solution of a number of experimental tests is compared against the measured hydrogen profiles. The test results supports the adequacy of the proposed model solution and also indicates that hysteresis and finite-rate kinetics should be kept in the model to predict the measured hydrogen concentrations.

Keywords: Hydrogen migration, Hydrogen disolution, Precipitation, Hydride blister, Zirconium alloys, Numerical modelling.

1 Introduction

Even at low concentrations, hydrogen often significantly changes the properties of the metals and their alloys. Embrittlement, a deleterious effect on the me-

chanical properties of a number of metals such as iron, titanium and zirconium can be a very complex process but it is related in general to the presence of hydrogen [43]; for instance, embrittlement of zirconium and its alloys may be explained by hydride precipitation [20][8][5][35].

In the specific case of the zirconium alloys used by the nuclear fuel industry, the hydrogen picked-up by the fuel cladding from that produced in the waterside corrosion reaction also impacts other performance properties such as corrosion resistance [46][11] and their dimensional stability [38] during normal operation and the performance during accident conditions [12][45]. Finally, hydrogen is the driving force of failure mechanisms such as Delayed Hydride Cracking [10][31]. Therefore, significant efforts have been carried out along the years to understand and to characterize the content and distribution of hydrogen in the corresponding industrial components [30].

Hydrogen is the smallest atom. Therefore, it may be expected to diffuse easily through metals. The hydrogen net flux depends on the existing concentration gradients but it is also assissted by thermal and hydrostatic stress gradients. Thus, extra terms should be added to the flux term due to concentration gradients, described by the Fick´s second law, to model the hydrogen migration inside a metal [34]. The advective nature of these extra terms will be shown later in this paper. Therefore, the thermal-hydrostatic stress assisted diffusion of hydrogen can be cast within the framework of the advection-diffusion equations and all the progress produced during the last years in the numerical solution of conservation laws is then available to solve this problem. However, the models developed in the past [16][19][47][13][4] do not take into account the advective-convective nature of the problem as they just add the thermal and stress extra terms to the concentration gradient to numerically solve afterwards the resulting transient equation.

Besides, the terminal solid solubility, TSS, of hydrogen is usually quite low in the range of temperatures of interest. Thus, the diffusion of hydrogen typically takes places in a two-phase, metal and metal-hydride, system. Furthermore, the density of the precipitated hydride is usually lower than the density of the base metal thus, the incremental volume of the hydride precipitate should be accomodated by elasto-plastic mechanisms by the surrounding matrix [28]. Due to this large, 11-16%, volumetric missfit strain, a hydrogen content higher than the concentration in equilibrium during dissolution is required to start precipitation on cooling down, *i.e.* the TSS is higher for precipitation than for dissolution [7][52][1][23]. This hysteresis effect along with the sluggish kinetics of hydride precipitation and dissolution [6] bring a source term into the conservation equation. This source term indicates that, physically, hydrides act as a source, or a sink, of the hydrogen in solution. However, most of the existing models do not incorporate either the hysteresis effect and/or the finite-rate kinetics.

Therefore, this paper presents first a derivation of a mathematical model of hydrogen diffusion in a two-phase, metal and metal-hydride, matrix incorporating the TSS hysteresis and finite-rate kinetics. It is shown that this equation can be written as an advection-diffusion equation with sources. To support some of the simplifications, available knowledge on the properties of the Zr-H system

is used. The resulting conservation equation is numerically solved by splitting it into an advection-diffusion equation and an ordinary differential equation, ODE, for the source term [49].

Within the methods based on the Finite Element Method already available to solve the advection-diffusion equation, see for instance references [51][37] for a review, the authors proposal is to use the well proved Two-Step Taylor Galerkin method [36]. As regards the source term, the formulation proposed for the rate of hydride precipitation and dissolution is based on over- and under-saturation and it will be integrated analytically, avoiding the numerical solution of the ODE.

Finally, performance of the proposed method is checked using a number of experimental cases of hydrogen migration in zircomium alloys incorporating precipitation and dissolution of zirconium hydrides. In this way, a number of key features of this process can be pointed out.

2 Mathematical Model

The zirconium-hydrogen phase diagram [44], Figure 1, indicates that in the range of temperatures, from room temperature to 550 ^{o}C, and hydrogen concentrations of interest, two phases may exist, α-Zr and δ-hydrides. Therefore, the total amount of hydrogen, M, in a representative volume, $d\Omega$, is

$$M = M_\alpha + M_\delta \tag{1}$$

Defining the volume fraction of hydrides, f, as the relative volume occupied by the δ-hydrides respective to the total volume

$$f = \frac{d\Omega}{d\Omega_\delta} \tag{2}$$

and the respective concentrations, C_α and C_δ, the total concentration of hydrogen, C, may be written as

$$C = (1 - f)\, C_\alpha + f\ C_\delta \tag{3}$$

Mass conservation requires that the rate of change of the total hydrogen concentration in any arbitrary volume Ω, equals the hydrogen flux, $\bar{\mathrm{J}}$, through the boundary, Γ

$$\frac{d}{dt}\int_\Omega C d\Omega = -\int_\Gamma \bar{J} \bullet \bar{n}\ d\gamma \tag{4}$$

As the arbitrary control volume Ω remains fixed, application of the divergence theorem allows the derivation of the differential conservation equation

$$\frac{dC}{dt} = -div\ \bar{J} \tag{5}$$

where the total flux in the α-Zr/δ-hydride composite is given by the weighted sum of the partial fluxes in each phase

$$\bar{J} = (1 - f)\, \bar{J}_\alpha + f\ \bar{J}_\delta \tag{6}$$

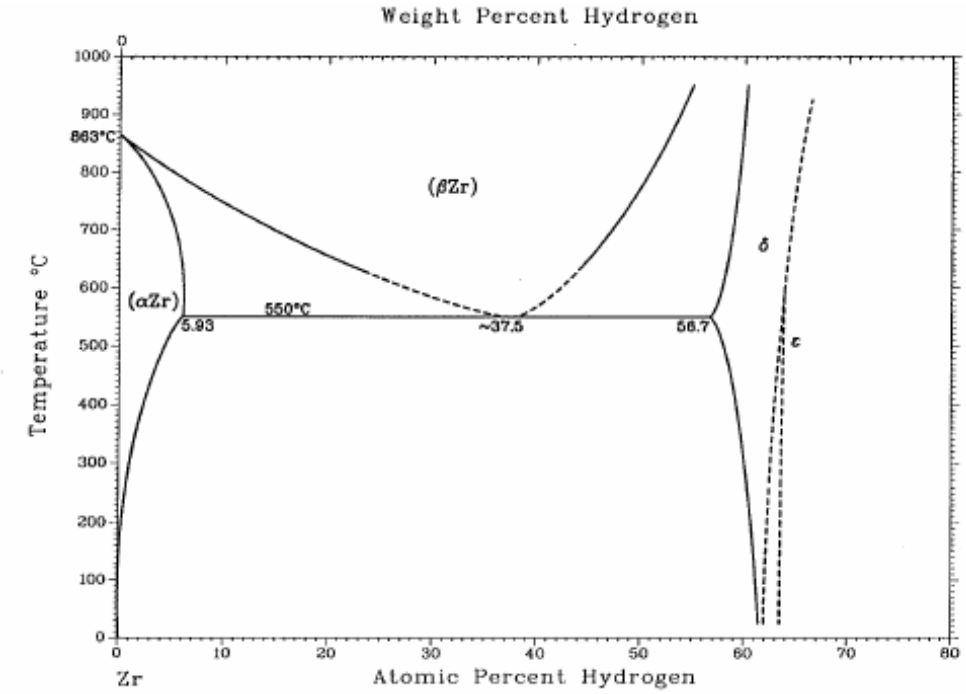

Figure 1: Zirconium-Hydrogen phase diagram

2.1 Flux of a solute in a stressed metal under thermal and concentration gradients

The flux of a solute under a force, $\bar{\mathrm{F}}$, is proportional to the mean diffusion velocity $\bar{\mathrm{v}}$ [34] of the affected atoms

$$\bar{J} = C\ \bar{v} \tag{7}$$

which, in turn, is proportional to the force on the particles

$$\bar{v} = M\ \bar{F}$$

where the mobility, M, is related to the diffusion coefficient by

$$M = \frac{D}{RT}$$

Considering a thermodynamic force derived from the chemical potential μ of the solute in the metal

$$\bar{F} = -grad\ \mu$$

then

$$\bar{J} = -\frac{DC}{RT}\ grad\ \mu \tag{8}$$

The chemical potential, μ, of a solute B in an ideal or dilute solution in a stress free condition may be written as (Raoult´s law)

$$\mu^B = \mu^{ref} + RT\ \ln(C)$$

where μ^{ref} is the chemical potencial in a reference state and the classical first Fick´s law is now obtained

$$\bar{J} = -D\ grad\ C$$

However, in a stressed metal the chemical potential of a mobile component B may be written as [21]

$$\mu^B = \mu^0 + \left.\frac{\partial w}{\partial N^B}\right|_{\sigma,T} - W$$

where μ^0 is the chemical potential of B under stress-free conditions, N^B is the number of B moles, the second term represents the strain energy of the solid per mole of B added and W is the work performed by the existing stress field per mole of addition of B.

Then, considering a material volume V under uniform stress

$$\frac{\partial w}{\partial N^B} = \frac{\partial}{\partial N^B}\left(\int^{\boldsymbol{\varepsilon}} V\boldsymbol{\sigma}\bullet d\boldsymbol{\varepsilon}\right) = \int^{\boldsymbol{\varepsilon}} \frac{\partial V}{\partial N^B}\boldsymbol{\sigma}\bullet d\boldsymbol{\varepsilon} = \bar{V}^B w$$

where $\bar{V}^B$ is the partial molal volume of B and it has been assumed that the compliance tensor is not affected by the addition of B.

The work performed by the applied stress field per mole of addition of B in the volume V is given by

$$W = V\boldsymbol{\sigma}\bullet\frac{\partial\boldsymbol{\varepsilon}}{\partial N^B} = V\ \sigma_{ii}\frac{\bar{V}^B}{3\ V} = \frac{1}{3}\sigma_{ii}\bar{V}^B$$

where it has been assumed that the deformation induced by the addition of B is purely volumetric.

Thus, the chemical potential of a solid solution of B under stress is

$$\mu = \mu^0 + \bar{V}^B\left(w - \frac{1}{3}\sigma_{ii}\right)$$

Inspection of this equation indicates that the strain energy w is of the order of σ^2/E, where E is the elastic moduls of the metal and the second term is of the order of σ.Therefore, the first term may be neglected, resulting in the often used equation [48][19]

$$\mu = \mu^0 - \bar{V}^B\frac{1}{3}\sigma_{ii} \tag{9}$$

Now, the more general case of migration under a temperature and a concentration gradient may be analyzed considering the phenomenological equations for heat, $\bar{\mathrm{J}}_q$, and mass, $\bar{\mathrm{J}}_B$, flux

$$\bar{J}_B = -L_{BB}\ grad\ \mu - L_{Bq}\ \frac{1}{T}grad\ T \tag{10}$$

$$\bar{J}_q = -L_{qB}\ grad\ \mu - L_{qq}\ \frac{1}{T}grad\ T \tag{11}$$

where the thermodynamical force for the energy flux is

$$\bar{F}_q = -\frac{1}{T}grad\ T$$

Using this selection of forces, the product of the forces and corresponding fluxes results in (temperature)(entropy)/(time)(volume) and the Onsager reciprocal relations, $L_{Bq} = L_{qB}$, applies [34]. However, other set of thermodynamic forces, and fluxes, may be used [41].

Equation (10) may be written also as

$$\bar{J}_B = -L_{BB}\ \left(grad\ \mu + \ \frac{L_{Bq}}{L_{BB}}\frac{1}{T}grad\ T\right)$$

and by comparison with equation (8)

$$L_{BB} = \frac{DC}{RT}$$

The ratio between the phenomenological coefficients, L_{Bq}/L_{BB}, is the heat of transport, Q^*. In the case the diffusion takes place under isothermal conditions, grad T=0, and the ratio of the heat and mass flux

$$\frac{\bar{J}_q}{\bar{J}_B} = \frac{L_{qB}}{L_{BB}} = Q^*$$

provides the physical interpretation of the heat of transport as the heat flux per unit flux of component B in the absence of a temperature gradient.

Therefore, the flux of a component B under a concentration, temperature and stress gradient may be written as

$$\bar{J}_B = -\frac{DC}{RT}\left(grad\ \mu^0 - \bar{V}_B\ grad\left(\frac{1}{3}tr\ \boldsymbol{\sigma}\right) + \frac{Q^*}{T}grad\ T\right)$$

or, also,

$$\bar{J}_B = -D\left(grad\ C - \frac{\bar{V}_B C}{RT}grad\ \left(\frac{1}{3}tr\ \boldsymbol{\sigma}\right) + \frac{Q^* C}{RT^2}grad\ T\right)$$

2.2 Precipitation and dissolution

Therefore, the flux of hydrogen through each phase i, under concentration, temperature and stress gradients may be written as [21][34]

$$\bar{J}^i = -D\left(grad\ C_{ss} + \frac{Q^*}{R}\frac{C_{ss}}{T^2}grad\ T - \frac{\bar{V}^H C_{ss}}{RT}grad\ \sigma_H\right)\Bigg|^i \qquad (12)$$

where

- D is the diffusion coefficient.
- C_{ss} is the concentration of hydrogen in solid solution in each phase.
- Q^* is the heat of transport of hydrogen in the corresponding matrix.
- R is the gas constant (8.314 J/K/mol).
- T is the temperature.
- $\bar{V}^H$ is the partial molal volume of hydrogen dissolved in each matrix: metal or hydride.
- σ_h is the hydrostatic component of the stress tensor,1/3 tr $\boldsymbol{\sigma}$.

In addition to diffusion through the metal lattice as an interstitial, or by vacancies, higher diffusivity paths such as dislocations or grain boundaries may exist [34]. A simple solution to incorporate the high diffusivity paths may be to considered an effective diffusion coefficient which incorporates the enhanced diffusivity [35].

In general, each phase may contain a movable hydrogen that can migrate under thermodynamical forces and a non-movable hydrogen [22]. As hydrogen in the $\alpha-$phase is in solid solution, it is customary to consider that this hydrogen can migrate through the metal lattice while the $\delta-$phase may contain either movable, in solid solution, and non-movable, molecular, hydrogen. Thus, the non-movable hydrogen concentration in the δ-phase can be determined from

the phase-diagram. As regards the hydrogen in solid-solution in the $\delta-$phase, Freund *et al.* [47] assumed that it obeys the following equation of state

$$C_{\delta}^{ss} = c\, C_{\alpha}^{ss} \tag{13}$$

where c may depend on temperature, at least for temperatures higher than 450^{o}C. Besides, these authors showed that the function c is related to the jump of the free hydrogen concentration at the phase-to-phase interfaces and used c=0.01 in their examples of application. Other authors, Markowitz [22] and Sawatzky [3], considered that all the hydrogen in the hydride phase is movable.

Then there are three unknowns C, C_{α}^{ss} and f in the system of equations (5), (6) and 12. However, they are related by the lever-rule equation (3) and by the phase transformation equation. Precipitation of the hydrogen in solid solution and dissolution of the existing hydrides are rather slow processes [7][6][23] and, as it will be shown later, this is a key feature to explain a number of experimental observations. Therefore, if the problem at hand involves either precipitation or dissolution, finite rate kinetics rather than the equilibrium conditions described by the phase diagram should be considered.

The rate of change of the hydride fraction may be written as

$$\frac{df}{dt} = \frac{\alpha^2 \left(1-f\right)^p}{C_{\delta} - C_{\alpha}} F\left(C_{\alpha}\right) \tag{14}$$

where

- α^2 is the precipitation/dissolution parameter. As it will be shown later, see equation (43) below, its inverse is proportional to the time constant of the precipitation/dissolution process. Considering that the rate of change of the hydride phase is a thermally activated process, α will be a function of temperature: $\alpha^2 = \alpha_0^2\, e^{-\frac{2\,Q_R}{RT}}$. In principle, α^2 may be different for precipitation and dissolution. Instantaneous kinetics, *i.e.* equilibrium conditions are achieved as $\alpha \rightarrow \infty$.The interested reader can consult Shewmon [33] and Marino [15] for further details on the meaning of α.

- the exponent p depends on the geometric distribution of the hydrides and

- the function F(C_{ss}) measures the degree of over or undersaturation of the α-phase

$$F(C_{\alpha}) = \begin{cases} C_{\alpha} - TSS_{PR} & \text{if } C_{\alpha} \geq TSS_{PR} \\ 0 & \text{otherwise} \\ C_{\alpha} - TSS_{D} & \text{if } C_{\alpha} < TSS_{D} \text{ and } f\ >\ 0.0 \end{cases} \tag{15}$$

  indicating that the rate of change of the hydride fraction is proportional to the distance to the precipitation/dissolution solvus. From the physical point of view, indicates the number of solute atoms entering into the precipitate. When the hydrogen concentration in solid solution is between the precipitation, TSS_{PR}, and the dissolution, TSS_{D}, solvus the hydride

fraction will not change *i.e.* hydrogen will not precipitate or existing hydrides will not dissolve. This function is equivalent to the loading function found, for instance, in the description of viscoplastic materials [25].

This system of equations should be complemented by the appropriate boundary conditions, either a fixed hydrogen concentration or a hydrogen flux through the boundary and, also, by the corresponding initial conditions for the unknowns.

2.3 Particularization to Zr-H system

The above system of equations may be simplified by considering the material properties involved as well as actual values for some of the variables, such as the hydride volume fraction and temperature. Therefore, the next section compiles the values of the relevant material properties that will be used afterwards to simplify the derived mathematical model.

2.3.1 Material properties

Molal volume of hydrogen As regards the molal volume of hydrogen in the $\alpha - Zr$ phase, $\bar{\mathrm{V}}^H$, a value of 7x10^{-7} m^3/mol is reported in [24][9] and 16.7x10^{-7} m^3/mol in [42]. This later value is confirmed in [39].

The value of the molal volume of hydrogen in the δ-hydride is 14x10^{-7} m$^3/mol$ accordding to Ells[9]. This value is reasonably close to the $\bar{\mathrm{V}}^{hyd}$ =16.7x10^{-7} m^3/mol as expected from other systems involving transition metals such as Nb-H[19].

Terminal solid solubility Two main references determining both the equilibrium solvus for the $\alpha - Zr$ in a consistent way are Kammenzind *et al.* [7] for Zircaloy-4 and Une *et al.*[23] for Zircaloy-2. Figure 2 depicts these solvus. Dashed lines indicate an extrapolation from the experimental data measured by each author. It should be pointed out that there are not significant differences between both proposals thus, between Zircaloy-2 and Zircaloy-4. The latter conclusion was also obtained by McMinn *et al [1].* This latter author determined the TSS$_{PR}$ and TSS$_D$ as well, concentrating their effort in the lower range of temperatures, T<300^{o}C. Although their TSS$_D$ matches that from the former authors, the TSS$_{PR}$ is significantly lower than that measured by Une and the extrapolation of the Kammenzind one.

The equations describing these solvus are

$$\text{Kammenzind} \begin{cases} \text{TSS}_{PR} = 3.1\ 10^4 e^{-\frac{3019}{T}} \\ \text{TSS}_D = 6.6\ 10^4 e^{-\frac{3845}{T}} \end{cases} \text{ ppm}$$

$$\text{Une} \begin{cases} \text{TSS}_{PR} = \max\left(5.26\ 10^4 e^{-\frac{3376}{T}}; 1.0710^4 e^{-\frac{2528}{T}}\right) \\ \text{TSS}_D = 1.28\ 10^5 e^{-\frac{4395}{T}} \end{cases} \text{ ppm}$$

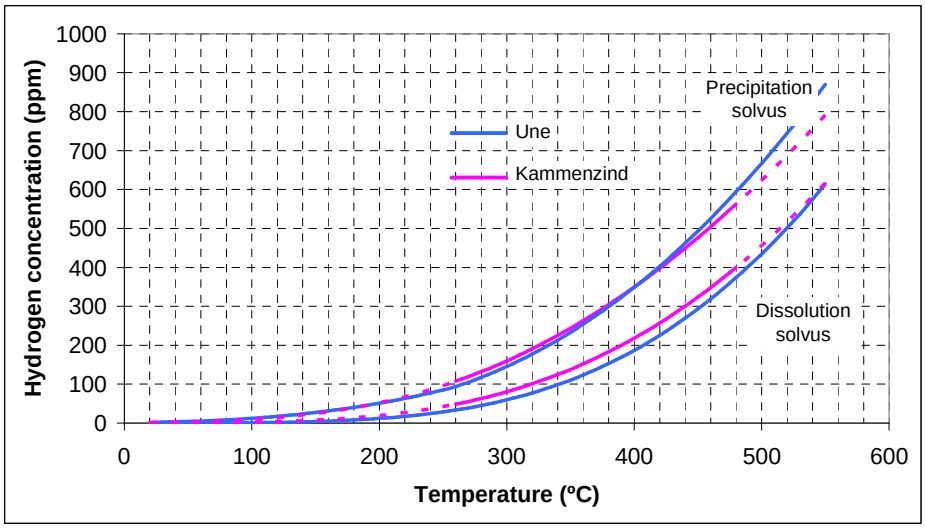

Figure 2: Terminal solid solubility of the alpha Zirconium from Kammenzind and Une.

As regards the $\delta-$hydride, the equilibrium solvus was determined by Libowitz [14] as

$$TSS_\delta = 1.66\ 10^4 - 3.74\ 10^4 e^{-\frac{2414}{T}}\ ppm$$

Diffusion coefficient The diffusion coefficient of the hydrogen in the $\alpha - Zr$ is available from Sawatzky [2] for Zircaloy-2 in the range of 260 to 560 ^{o}C

$$D\left(m^2/s\right) = 2.17\ 10^{-7}\ e^{-\frac{4190}{T}}$$

and for Zircaloy-4 from Kammenzind [7] in the range of 300 to 480 ^{o}C.

$$D\left(m^2/s\right) = 0.8\ 10^{-7}\ e^{-\frac{3978}{T}}$$

Kearns determined the diffusivity in Zircaloy-4 and Zircaloy-2 rolled sheet in the temperature range from 275 to 700 ^{o}C. He found no measurable differences between both materials. However, he found differences between the different directions in the sheet. His proposed the following diffusivity in the longitudinal, transverse and through-thickness directions

$$D_L\left(m^2/s\right) = 7.73\ 10^{-7}\ e^{-\frac{5415}{T}}$$

$$D_T\left(m^2/s\right) = 5.84\ 10^{-7}\ e^{-\frac{5145}{T}}$$

$$D_t\left(m^2/s\right) = 7.90\ 10^{-7}\ e^{-\frac{5365}{T}}$$

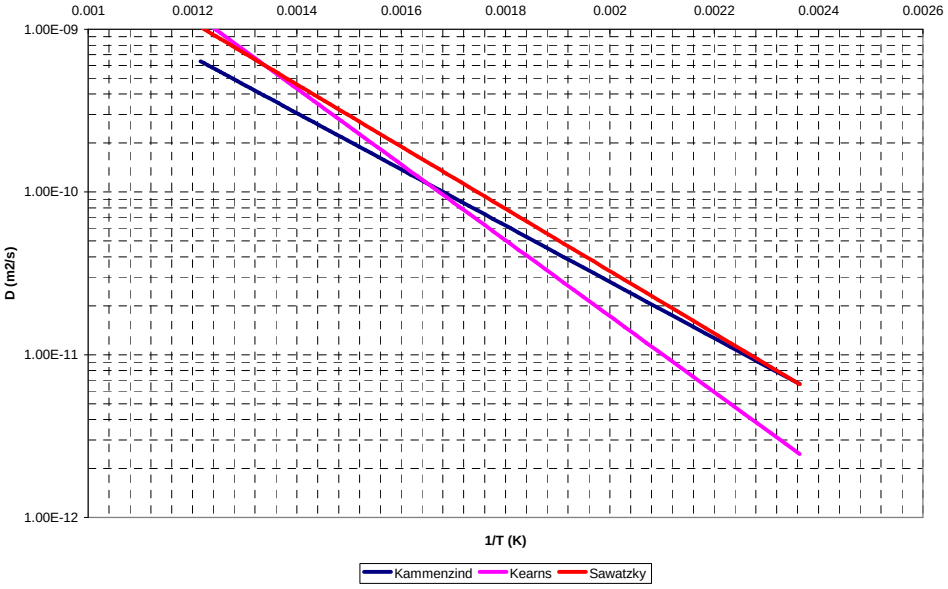

Figure 3: Diffusivity of the hydrogen in the alpha zirconium

Figure 3 depicts these three proposals. It is observed that at the higher temperatures, Kearns' and Sawatzky's proposals are similar while they are different at the lower temperature values where Sawatzky's and Kammenzind's proposal are closer.

Finally, the diffusion coefficient of hydrogen in the $\delta-$hydride is [3]

$$D\left(m^2/s\right) = 1.09x10^{-7}e^{-\frac{5730}{T}}$$

Heat of transport The heat of transport of hydrogen in the $\alpha - Zr$, Q^*_α, has been determined by Kammenzind [7] and by Sawatzky [40]. Kammenzind values on Zircaloy-4 ranged from 4.5 to 9 kcal/mole while Sawatzky proposed a value of 6.0 kcal/mole for Zircaloy-2.

As regards the heat of transport of hydrogen in the $\delta-$hydride phase, a value of $Q^*_\delta = 1.3$ kcal/mole has been used by Sawatzky [3].

Precipitation/dissolution parameters Marino [15][27] derived the following values for the precipitation rate constant, α^2 in equation (14),:

$$\begin{cases} \alpha^2 = 2.5e-5 \text{ sec}^{-1} \text{ for T}\leq 260^oC \\ \alpha^2 = 1.5326\ e^{-\frac{5878}{T}} \text{ sec}^{-1}\text{for T}> 260^oC \end{cases}$$

From his work on the hydrogen supercharging phenomenon, Marino concluded that a cutoff value for the reprecipitation constant should exist. At

sufficiently high temperatures, the $\delta-$phase precipitation is controlled by diffusion processes then, temperature dependent whereas at lower temperatures, the precipitation becomes martensitic and independent of temperature. Marino obtained a best fit to the data from Sawatzk's specimens by setting $\alpha_{\min} = 5.0\ 10^{-3}$.

Later, Kammenzind *et al.* [7] quantified the value of the precipitation rate constant in the temperature range from 288^{o}C to 360^{o}C, as

$$\alpha^2 = 5.76\ 10^4\ e^{-\frac{11537}{T}}\ \sec^{-1}$$

and, more recently, Une *et al.* [23] derived the following expression for the precipitation rate in the range from 181 ^{o}C to 380 ^{o}C:

$$H = 1.18\ 10^3 e^{-\frac{4296}{T}}\ ppm/\sec$$

These authors calculated the precipitation rate in a different way, from the precipitation duration and the degree of supersaturation that they regarded as the difference between the precipitation solvus and the solvus for hydride growth. Considering the expressions for these solvi derived by these authors, the precipitation rate constant can been calculated as

$$\alpha^2 = 1.1849\ e^{-\frac{2701}{T}}\ \sec^{-1}$$

It should be noted that at temperatures higher than 380^{o}C, a not-thermally activated behaviour in the precipitation rate was noticed by these authors, probably indicating a change of the kinetics mechanism from diffusion controlled to a different one. Figure 4 depicts the values for the precipitation rate constant accordding to the different authors and Figure 5, the corresponding hydrogen precipitation rates. It should be noticed that there are differences of several orders of magnitude in the precipitation rate between the three researchers.

Finally, it should be mentioned that as values for the redissolution constant are not available, as far as for the authors knowledge, the precipitation constant is also, initally, used for the redissolution process. In these regards, Kammenzind *et al.* initially considered that dissolution was instantaneous to, later on, conclude that dissolution is a rather slugish process [6] as shown in Section 4.3.

2.3.2 Model characteristics

As shown in the previous sections, the hydrogen conservation equation (5) may be written

$$\frac{dC}{dt} = -div\ \left[-\frac{D_\alpha C_\alpha^{ss}}{RT}(1-f)\left(grad\ \mu_\alpha^H + \frac{Q_\alpha^*}{T} grad\ T\right) - \right. \tag{16}$$

$$\left. - \frac{D_\delta\ c\ C_\alpha^{ss}}{RT}\ f\ \left(grad\ \mu_\delta^H + \frac{Q_\delta^*}{T} grad\ T\right)\right]$$

as it was used by Markowitz [22] and Sawatzky [3].

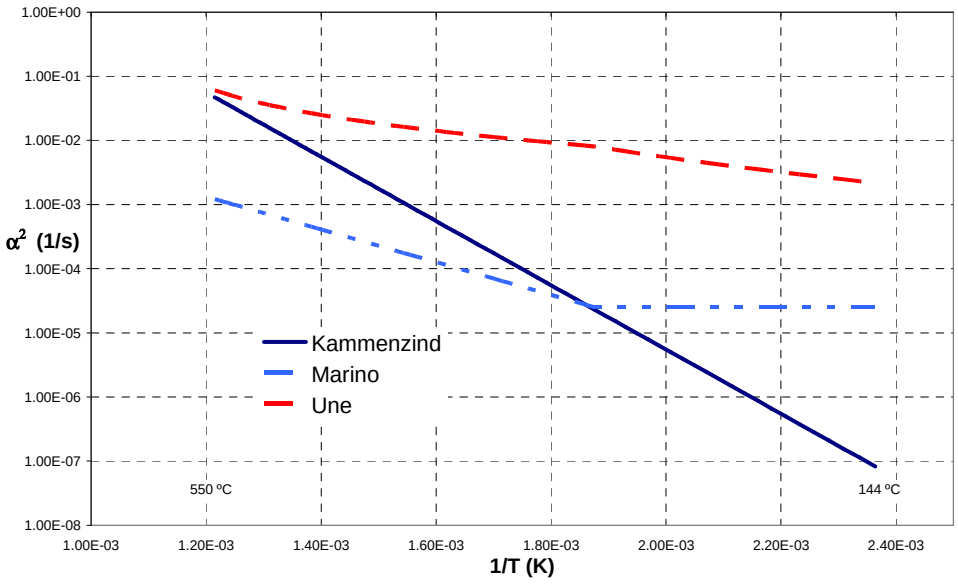

Figure 4: Precipitation rate constant as a function of tenmperature

From the material properties presented in the previous section, the ratio between the diffusivity through each phase can be calculated. Considering a reasonably high total hydrogen concentration of 6000 ppm for practical applications, this ratio is of the order of 20

$$\frac{D_\alpha\,(1-f)}{D_\delta\;f} \approx 20$$

and it is not balanced, but even increased, by the thermal component due to the different heat of transport $Q^*_\alpha/Q^*_\delta \approx 6$ which favours again diffusion in the $\alpha - Zr$.This ratio further increases as the hydrogen content reduces and the volume fraction of hydrides further reduces; for instance, for a total hydrogen content of 600 ppm, the ratio becomes 750 at 400 ^{o}C.

Finally, considering also the expected smaller hydrogen concentration in solid solution in the hydrides, in most practical applications diffusion through the $\delta-$hydrides may be neglected. However, as pointed out by Markowitz [22] as the volumetric hydride fraction increases, diffusion through the hydrides should be kept in the model equations.

Thus, neglecting the hydrogen diffusion through the $\delta-$phase, the hydrogen flux given by equation (6) is approximated by

$$\bar{J} = (1-f)\,\bar{J}_\alpha \tag{17}$$

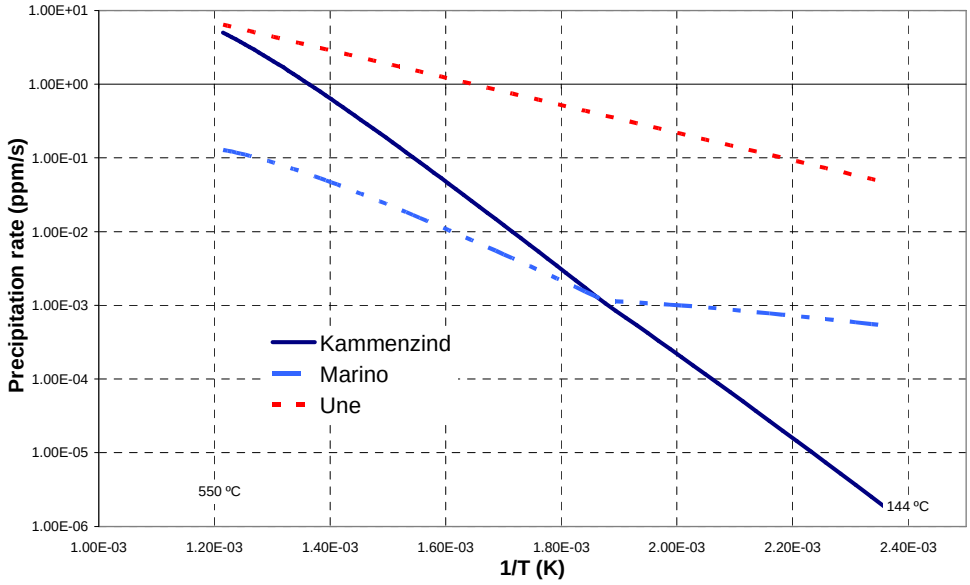

Figure 5: Precipitation rate as a function of temperature.

and the mass conservation equation becomes

$$\frac{dC}{dt} = -div\left[-\frac{D_\alpha C_\alpha}{RT}\left(1-f\right)\left(grad\ \mu_\alpha^H + \frac{Q_\alpha^*}{T} grad\ T\right)\right] \tag{18}$$

which is the form used by most authors [4][13][7].

Recalling now the expression for the chemical potential in stressed solids, equation (9),

$$\mu = \mu^0 - \bar{V}^H \sigma_h \tag{19}$$

the mass conservation equation may be written

$$\frac{dC}{dt} = -div\ \left[-D_\alpha\left(1-f\right)\left(grad\ C_\alpha + \frac{Q_\alpha^*}{R}\frac{C_\alpha}{T^2} grad\ T - \frac{\bar{V}^H\ C_\alpha}{RT} grad\ \sigma_h\right)\right] \tag{20}$$

or in a form more usual in the field of conservation equations as

$$\frac{dC}{dt} + div\ \left[-D_\alpha\left(1-f\right)\left(\frac{Q_\alpha^*}{RT^2} grad\ T - \frac{\bar{V}^H}{RT} grad\ \sigma_h\right) C_\alpha\right] = -div\ \left[-D_\alpha\left(1-f\right)\ grad\ C_\alpha\right] \tag{21}$$

It should be noticed that the coefficients

$$\begin{cases} D_\alpha\left(1-f\right)\frac{Q_\alpha^*}{RT^2} grad\ T \\ D_\alpha\left(1-f\right)\frac{\bar{V}^H}{RT} grad\ \sigma_h \end{cases}$$

have the dimensions of a velocity, (L/t), as it may be expected as the atoms flux is proportional to this velocity as already described by equation (7).

Besides, in most practical applications, such as in a thicked walled tube subjected to a pressure differential,

$$\frac{\frac{Q^*}{T} grad\ T}{\bar{V}^H\ grad\ \sigma_h} >> 1$$

considering the values of the material properties involved as well as grad σ_h is only relevant close to stress risers, such as at crack tips due to the induced singularity, the hydrostatic stress assissted hydrogen migration can be dismissed in lieu of the thermal gradient:

$$\frac{dC}{dt} + div\ \left[-D\,(1-f)\,\frac{Q^*}{RT^2} grad\ T\ C_\alpha\right] = -div\ \left[-D\,(1-f)\,grad\ C_\alpha\right] \quad (22)$$

Additionally, the mass conservation equation may be written as a function of C_α and f alone just by derivation of the lever rule equation (3) respective to time

$$\frac{dC}{dt} = (1-f)\,\frac{dC_\alpha}{dt} + (C_\delta - C_\alpha)\,\frac{df}{dt} \quad (23)$$

and incorporating equations (17) and (14)

$$(1-f)\,\frac{dC_\alpha}{dt} = -div\ \left[(1-f)\,\bar{J}_\alpha\right] - \alpha^2\,(1-f)^p\,F\,(C_\alpha) \quad (24)$$

Assuming that $f << 1$ and the above described simplifications, this equation can be written as proposed by most authors, such as Kammenzind [7],

$$\frac{dC_\alpha}{dt} = -div\ \left[(1-f)\,\bar{J}_\alpha\right] - \alpha^2 F\,(C_\alpha) \quad (25)$$

and

$$\frac{dC_\alpha}{dt} + div\left[-D\,(1-f)\,\frac{Q^*}{R}\,\frac{1}{T^2} grad\ T\ C_\alpha\right] = -div\ \left(-D\,(1-f)\ \ grad\ C_\alpha\right) - \alpha^2 F\,(C_\alpha) \quad (26)$$

Again, the thermally assisted migration of hydrogen can be cast as an advection-diffusion process with a source where

- the temperature gradient results in a hydrogen transport velocity equal to $\frac{Q^*}{RT}\frac{D}{T} grad\ T$: the advection component
- there is a pure diffusional component, $D\ grad\ C_\alpha$ obeying the second´s Fick law,
- the precipitation/dissolution of hydrides result in a sink/source of hydrogen of magnitude, $\alpha^2 F(C_\alpha)$.

and all the existing knowledge in the solution of advection-diffusion equations with sources can be used in its numerical solution.

Therefore, also three characteristic time constants exists:

- $t_{adv} = \frac{h}{D(1-f)\frac{Q^*}{R}\frac{1}{T^2} grad\ T}$ for the advection component
- $t_{dif} = \frac{h^2}{D(1-f)}$ for the diffusion and,
- $t_{rec} = \frac{1}{\alpha^2}$ for the (reaction) precipitation/dissolution

where h is a relevant distance and the examination of the ratios between these time constants provides signifcant insights into the dominant phenomena.

The first ratio that can be formed is the Peclet number

$$Pe = \frac{t_{dif}}{t_{adv}} = h\frac{Q^*}{R}\frac{1}{T^2} grad\ T = \frac{Q^*}{R}\frac{1}{T^2}\Delta T$$

that measures also the strength of the advection transport vs. the diffusion. Low values of the Peclet number indicates that the time constant of the diffusion process is smaller than the time constant of the advection process *i.e.*, diffusion is the dominant phenomenon. In the same way, adimensional numbers can be formed between the reaction and advection/diffusion time scales.

The following table presents the values of the time constants in the case of the thermally assisted transport of hydrogen in the radial direction of the 17x17 fuel cladding tube with thickness 570 μm presented in Section 4.4, considering a heat flux of 70 W/cm^2 and temperatures of 375 ^{o}C and 180 ^{o}C, the limits of validity of the precipitation rate parameter.

T (K)	648	453
k (W/mK)	17.02323	14.72223
Q* (cal/mol)	7000	
D (Kearns) (m^2/s) =	2.0 10^{-10}	5.7 10^{-12}
grad T(K/m) =	4.1 10^4	4.75 10^4
α^2 (Kammenzind)(1/s)=	1.1 10^{-3}	5.0 10^{-7}
α^2 (Marino)(1/s)=	1.72 10^{-4}	2.5 10^{-5}
α^2 (Une)(1/s)=	1.8 10^{-2}	3.0 10^{-3}
u(m/s) =	6.9 10^{-8}	4.6 10^{-9}
t_{adv} (s) =	8297	1.2 10^6
t_{dif} (s) =	1621	5.7 10^4
P_e =	0.20	0.46
$t_{precipt}$ (Kammnezind) (s) =	937	2 10^6
$t_{precipt}$(Marino) (s) =	5676	4. 10^4
$t_{precipt}$(Une) (s) =	55	328

Therefore, in the case of the cladding tube, diffusion slightly dominates over advection and would set the time step size in the numerical model. Besides, the time scale for precipitation based on Marino´s rate parameter are of the

same order of magnitude that the diffusion time scale. However, the time scale based on Une´s recommendation is much shorter than that for diffusion and will control the solution. Finally, the time scale for precipitation based on Kammenzind´s recommendation is similar or longer than that for diffusion. Therefore, it can be concluded that in this case, diffusion is the controlling phenomenon but modelling precipitation may require special provisions.

Finally, it is worthy to repeat this exercise on the specimens used in the experimental efforts to determine some of the material properties. As an example, next table summarizes the corresponding aparemeters and time scales for the Sawatzky´s specimen described in Section 4.2. the specimen length is 2.5 cm. It should be noted that the hotter end of the specimen, 477 ^{o}C, is above the range of applicability of the precipitation rate parameter and a change in the kinetics was observed by Une *et al* [23]. Therefore, the corresponding figures should be treated with care as actual precipitation rates may be lower than the calculated ones.

T (K)	750	403
Q* (cal/mol)	7000	
D (Kearns) (m^2/s) =	6.2 10^{-10}	5.7 10^{-12}
grad T(K/m) =	1.39 10^4	
α^2 (Kammenzind)(1/s)=	1.20 10^{-2}	2.13 10^{-8}
α^2 (Marino)(1/s)=	6.05 10^{-4}	2.50 10^{-5}
α^2 (Une)(1/s)=	3.23 10^{-2}	1.46 10^{-3}
u(m/s) =	5.34 10^{-8}	3.91 10^{-10}
t_{adv} (s) =	10680	1.46 10^6
t_{dif} (s) =	526	2.49 10^5
P_e =	0.05	0.17
$t_{precipt}$ (Kammnezind) (s) =	83	4.7 10^7
$t_{precipt}$(Marino) (s) =	1653	4.0 10^4
$t_{precipt}$(Une) (s) =	31	687

In this case, the diffusion time scale is even lower than in the previous case, this result attributed to the lower thermal gradient, and much lower than the advection time scale. Therefore, in this case, diffusion is the controlling mechanism and it sets the time step in the numerical model. Again, there is a wide variety of time scales for the precipitation process.

3 Numerical model

The solution scheme proposed in this work mimics the physics of the underlying process. In the first step, the advection-diffusion equation (22) is solved using the previous step results in order to obtain the new value of C^{n+1}. Then, the phase change kinetics are incorporated into the solution using the calculated dC/dt to solve (24) and (3).

From the numerical point of view, with reference to equation (26), this is an splitting procedure where the pure advection-diffusion equation is solved first

$$\frac{dC_\alpha}{dt} = -div\ \bar{J} \tag{27}$$

to calculate C_α^{adv} and, then, the source is incorporated by solving an ordinary differential equation

$$\frac{dC_\alpha}{dt} = -\alpha^2 F\left(C_\alpha\right) \tag{28}$$

with initial condition $C_\alpha = C_\alpha^{adv}$. This method allows the combination of optimum schemes for the solution of the advection-diffusion and for the ODE [50] and it is recommended for strong sources [26]. Next sections describe the methods proposed to solve each step.

3.1 First step: advection-diffusion

The advection-diffusion equation describing the thermally assisted diffusion of hydrogen

$$\frac{dC}{dt} + div\ \left[-D\left(1-f\right)\frac{Q^*}{R} grad\left(-\frac{1}{T}\right) C_\alpha\right] = -div\ \left[-D\left(1-f\right) grad\ C_\alpha\right]$$

can be discretized and solved using any of the numerous available algorithms, see for instance [51][17]. All of them present advantages and disadvantages when compared to the others. From these methods, those based on the Lax-Wendroff scheme have demonstrated a good compromise between accuracy and computational efficiency. Therefore, the authors' choice is the second order Two-Step Taylor-Galerkin. References describing this algorithm and its numerical implementation abound. The interested reader is referred to [36][51] and references there in for general details. The application of the algorithm to the problem at hand is included in the present paper.

The Taylor-Galerkin procedure for solving the conservation equation

$$\frac{\partial C}{\partial t} + div\bar{F} + div\,\bar{G} = 0 \tag{29}$$

where $\bar{F}$ is the advective flux and $\bar{G}$ is the diffusive flux, starts from a second order expansion in time

$$C^{n+1} = C^n + \Delta t\ \frac{\partial C}{\partial t}\bigg|^n + \frac{1}{2}\Delta t^2\ \frac{\partial^2 C}{\partial t^2}\bigg|^n \tag{30}$$

where the first order time derivative of the unknowns can be calculated using equation (29)

$$\frac{\partial C}{\partial t}\bigg|^n = \left(\text{-}div\ \bar{J}\right)^n \tag{31}$$

To obtain the second order time derivative, the Two-Step Taylor-Galerkin procedure considers an intermediate step between t^n and t^{n+1}. The aim of this first time step is to calculate the solution at a time $t^{n+1/2}$. This step is followed by a second one that brings the solution to t^{n+1}. Most of the times, the flux vector at $t^{n+1/2}$ is calculated ignoring the contribution of the diffusive flux.

In this way, the first step results in

$$C^{n+1/2} = C^n + \frac{\Delta t}{2}\left(-div\,\bar{J}^n\right) \tag{32}$$

which allows the calculation of $\bar{J}^{n+1/2}$.

The flux vector is a function of the concentration of hydrogen in solid solution, C_α, and the hydride fraction, f. Therefore, the corresponding values should be calculated at $t^{n+1/2}$ from the total hydrogen concentration, $C^{n+1/2}$. However, the calculation of $C_\alpha^{n+1/2}$ and $f^{n+1/2}$ requires considering the phase-change. This is done as explained in the next section. Then, $\bar{J}^{n+1/2}$, can be calculated.

Considering now a Taylor series expansion of the flux term,

$$\bar{J}^{n+1/2} = \bar{J}^n + \left(\frac{\partial \bar{J}}{\partial t}\right)^n \frac{\Delta t}{2} \tag{33}$$

the flux time derivatives is

$$\left(\frac{\partial \bar{J}}{\partial t}\right)^n = \frac{2}{\Delta t}\left(\bar{J}^{n+1/2} - \bar{J}^n\right) \tag{34}$$

Incorporating these expressions into the second order time derivative

$$\left.\frac{\partial^2 C}{\partial t^2}\right|^n = \frac{\partial}{\partial t}\left(\text{-}div\,\bar{J}\right)^n \tag{35}$$

results in

$$\left.\frac{\partial^2 C}{\partial t^2}\right|^n = \frac{2}{\Delta t} - div\left[\left(\bar{J}^{n+1/2} - \bar{J}^n\right)\right] \tag{36}$$

Now replacing the expressions for the first and second order time derivatives in the Taylor series expansion (30) allows the determination of the C^{n+1}

$$C^{n+1} = C^n + \Delta t\left(-div\,\bar{J}^{n+1/2}\right) \tag{37}$$

This equation is spatially discretized using conventional Galerkin weigthing to finally result in the system of equations to be solved to obtain the increment of the nodal total hydrogen concentration during the time step:

$$\frac{1}{\Delta t}\int_\Omega N^i N^j d\Omega\,\Delta C^j = \int_\Omega \bar{J}^{n+1/2} \bullet grad\,N^i\,d\Omega - \int_{\Gamma_N} N^i\,\left(\bar{J}^{n+1/2}\cdot\bar{n}\right)\,d\gamma \tag{38}$$

or, in matrix form,

$$\frac{1}{\Delta t}\mathbf{M}\,\Delta\bar{C} = \int_\Omega \mathbf{B}\bar{J}^{n+1/2} d\Omega - \int_{\Gamma_N} \bar{N}\,\left(\bar{J}^{n+1/2}\cdot\bar{n}\right)\,d\gamma \tag{39}$$

where

- **M** is the mass matrix
- **B** is the matrix of spatial derivatives of the shape functions N^i
- $\bar{N}$ is the vector of shape functions $\left\{N^i\right\}$
- $\Delta\bar{C}$ is the vector of nodal increments of the total hydrogen concentration $\left\{\Delta C^i\right\}$

3.2 Phase change

Once the values of the nodal total concentration of hydrogen, C^{n+1}, have been calculated as shown above, the derivation respective to time of the lever rule and the phase change equation results

$$(1-f)\,\frac{dC_\alpha}{dt} = \frac{dC}{dt} + \alpha^2\,(1-f)^p\,F\,(C_\alpha) \tag{40}$$

Now assuming that the hydride fraction, *f,* remains constant through the time step, and considering the definition of $F\,(C_\alpha)$, equation (15), this differential equation can be integrated analytically, resulting

$$C_\alpha^{n+1} = TSS_{PR} + (C_\alpha^n - TSS_{PR})\;\; e^{-\Delta t/\tau} + \frac{\tau}{(1-f)}\;\frac{\Delta C}{\Delta t}\bigg|^n \left(1 - e^{-\Delta t/\tau}\right) \tag{41}$$

$$C_\alpha^{n+1} = TSS_{D} + (C_\alpha^n - TSS_{D})\;\; e^{-\Delta t/\tau} + \frac{\tau}{(1-f)}\;\frac{\Delta C}{\Delta t}\bigg|^n \left(1 - e^{-\Delta t/\tau}\right) \tag{42}$$

when precipitation/dissolution respectively takes place and where a time constant of the precipitation/dissolution process is defined as

$$\tau = 1/\left[\alpha^2\,(1-f)^{p-1}\right] \tag{43}$$

Once C_α^{n+1} has been obtained, the updated hydride fraction can be calculated using the lever rule equation

$$f^{n+1} = \frac{C^{n+1} - C_\alpha^{n+1}}{C_\delta - C_\alpha^{n+1}}$$

The assumption made for f to remain constant through the time step is quite plausible as f changes are much more sluggish than C_α, *i.e.* considering the large amount of hydrogen concentration in the δ-hydride, of the order of 16000 ppm, small changes in the hydride fraction produce rather large changes in the solid solution concentration.

The second assumption made in this derivation is that precipitation or dissolution takes place during the complete time step *i.e.* the corresponding solvus is not crossed during a time step. Although compliance with this requirement will not hold in general, the limits imposed in the maximum hydrogen change

during a time step, for instance 2.5 ppm [4], to maintain overall accuracy will keep bounded this type of error.

In the case one consider necessary to maintain a very high accuracy when solving the phase change equation (40), it can be also solved numerically using, for instance, a fourth-order Runge-Kutta. The fourth order Runge-Kutta has shown to be very robust when applying the splitting procedure in the solution of problems involving strong sources [26], however, one should also keep in mind the corresponding computational cost. Application of the Two-Step Taylor Galerkin to the source term is highly not recommended in view of the results presented in [26].

In the case $F(C_a) = 0$, there is no change in the hydride fraction $f^{n+1} = f^n$ and the new concentration in solid solution is calculated using the lever rule

$$C_\alpha^{n+1} = \frac{C^{n+1} - f^n \, C_\delta}{1 - f^n} \tag{44}$$

If the limit $f = 1$ is reached, the above derivation is not applicable as only one phase, δ-hydride, exists and the lever rule reduces to C=C_δ and this step is not necessary.

Finally, the reader would already noticed that the phase-change equation is solved locally, at each mesh node, without any spatial discretization of the phase-change equations. Therefore, the proposed approach is computationally very efficient.

3.3 Algorithmic Aspects

3.3.1 Equation system solution

A system of equations

$$\underline{\mathrm{M}}\mathbf{x} = \mathbf{f} \tag{45}$$

can be economically solved using a Jacobi iteration scheme

$$\mathbf{x}^{(k+1)} = \mathbf{x}^{(k)} + M_L^{-1} \left(\mathbf{f} - \underline{\mathrm{M}}\, \mathbf{x}^{(k)} \right) \tag{46}$$

where the superscript k is the iteration counter, if an approximate inverse matrix, M_L^{-1}, is known in advance.

As in the case of (38) an approximate inverse of the system matrix, $\underline{\mathbf{M}}$**,** is the lumped mass matrix, the equation system (38) can be solved using this algorithm. Typically, less than six iterations are enough to obtain an accurate solution.

3.3.2 Allowed time step

The algorithm proposed to solve the advection-diffusion step is conditionally stable. To ensure the stability of the Taylor-Galerkin scheme, the Courant

number, C_n, has to fulfil the condition [36]

$$C_n \leq f_s \left(\sqrt{\frac{1}{Pe^2} + \beta} - \frac{1}{Pe} \right) \tag{47}$$

where

- f_s is a safety factor typically taken between $0.8 \div 0.95$,
- $C_n = \frac{\left| D(1-f) \frac{Q^*}{R} grad\left(-\frac{1}{T}\right) \right|}{h_e / \Delta t}$
- $Pe = \frac{\left| D(1-f) \frac{Q^*}{R} grad\left(-\frac{1}{T}\right) \right|}{D(1-f)} h_e = \left| \frac{Q^*}{R} grad\left(-\frac{1}{T}\right) \right| h_e$ is the element Peclet number
- $\beta = 1$ in the case $\underline{\mathrm{M}}$ is the lumped mass matrix and $\beta = 1/\sqrt{3}$ for the consistent mass matrix,
- h_e is a typical element length.

Thus, the advection-diffusion step places the following constrain in the allowable time step

$$\Delta t \leq f_s \left(\sqrt{\frac{1}{Pe^2} + \beta} - \frac{1}{Pe} \right) \frac{h_e}{\left| D\left(1-f\right) \frac{Q^*}{R} grad\left(-\frac{1}{T}\right) \right|} \tag{48}$$

It has to be pointed out that in order to improved the accuracy and smooth out of oscillations [29] the calculation of the unknowns at time $t^{n+1/2}$ performed at the element level, equation (32), uses the optimum time step value given by equation (48). This optimum value is calculated and used for each element in turn, while the minimum of the time steps calculated for the whole mesh, is used in (38) to ensure overall scheme stability.

From this discussion, it is clear that lumped mass matrix produces a longer allowable time step as well as minimizes the computational effort to solve the system of equations. Although some criticism has been risen on the lumped mass matrix approach [37], the results obtained by the authors using the lumped mass matrix compare in accuracy with those obtained using the consistent mass matrix approach while the computational effort was greatly reduced when using the lumped mass matrix. Therefore the lumped mass matrix is the authors' preferred choice.

Furthermore, if one is only interested in the steady-state results but not in the transient, the local time stepping, *i.e.* use the lumped mass matrix and the optimum time step given by (48) for each node, is advocated as it accelerates convergence to steady-state [51]. However, in the authors experience, this procedure does not always preserve the total hydrogen in the discretized spatial domain. The reasons for this lack of hydrogen conservation are not clear and this procedure is not recommended.

Finally, for accuracy reasons, the time step is also limited by the amount of total hydrogen change during the time step [4]. Typical values tested by the authors range from 1 to 3 ppm.

3.3.3 Delta-hydride limit

In the limit case when the control volume is completely occupied by the $\delta-$phase, *f=1,* as it has been assumed that hydrogen does not migrate through the $\delta-$phase in the model equations derivation, the hydrogen flux will be null

$$\bar{J} = (1 - f)\, \bar{J}_\alpha = \bar{0} \tag{49}$$

and the total hydrogen concentration fixed at C_δ as f$\not>$ 1.

Compliance with this equation is achieved on a local, point, basis or, element wise if all the nodes fulfills the condition $f = 1$ as f at the quadrature points will be also unity and then, the calculated flux, null. However, if for some nodes of the element $f < 1$ then, the calculated flux at the quadrature points will be no null and so, the integrated flux. Therefore, according to equation (39), all the nodes in the element, even those with $f = 1$, will have a no null total concentration increment and, consequently, the condition f$\not>$1 will be not fulfilled in those nodes.

The procedure used to overcome this problem, while preserving the total hydrogen content in the modeled solid, is just to split the element integrated flux

$$\int_{\Omega_e} \bar{J}^{n+1/2} \bullet grad\, N^i \, d\Omega \tag{50}$$

only between those nodes in the element with $f < 1$.

4 Test cases

This section presents the results obtained in a number of tests cases that support the adequacy of the proposed model as well as to point out the key features of the thermal assisted diffusion of the hydrogen in zirconium alloys. There are further experimental data available but most of the times the information available is uncomplete and can not be used for the intended purpose.

4.1 Planman's specimen

The first example checks the proposed model adequacy to reproduce the measured hydrogen profile in a Zr-2 tubing sample precharged with hydrogen under a thermal gradient. This experiment was carried out by Planman and Freund and the interested reader is referred to [47] for further details.

The sample was obtained by cutting a Zr-2 tubing to a length of 4 cm and then, chemically preloaded with 455 ppm oh hydrogen. Finally, it was annealed in an air furnace to induce the hydrogen redistribution in the axial tube direction. The temperature at the colder and hotter end of the sample was

64 ^{o}C and 418 ^{o}C respectively *i.e.* the thermal gradient was 88.5 ^{o}C/cm. After anealing the sample for 25 days, the hydrogen concentration was measured on different cladding rings using melt extraction. It should be pointed out that steady-state conditions were not reached after 25 days and thus, the phase change kinetics can be checked using this experiment.

Considering the sample preparation and the solubility limits described in Section 2.3.1, all the hydrogen before the annealing basically should be as a $\delta-$hydride because the solubiltiy limit is quite low at room temperature, of the order of a few ppm. Assuming that the rise to the annealing temperature is much shorter that the time needed for hydride dissolution, the hydrogen as δ-hydride will remain during the heat-up and then, it will start dissolving to increase the hydrogen in solid solution to the TSS_D.

This hydrogen profile after annealing was measured by melt extraction after cutting the specimen in eight rings of equal length. Figure 7 depicts the measured hydrogen in each ring. It should be point out that the total hydrogen in the specimen calculated from this profile is remarkably equal to the initial one, existing in the specimen before annealing.

Figure 6 depicts the initial hydrogen concentration as δ-hydride calculated at room temperature using the TSS_{PR} from Kammenzind and the corresponding TSS_D along the sample. It is clear that at the hotter end, at the right side, the initially existing hydrides will be dissolving to achieve the corrsponding equilibrium TSS_D while, as the TSS_D in the cold end is very low, they will remain fundamentally undissolved. Finally, the hydrogen becoming in solid solution due to the hydride dissolution will migrate to the colder, left, sample end due to the imposed thermal gradient thus, devoiding the hotter end from hydrogen in solid solution and continuing the hydride dissolution.

For modelling purposes, the specimen has been spatially discretized using 133 linear elements of equal length. With reference to Section 2.3.1, the terminal solubility solvus, TSS_{PR} and TSS_D, are taken from Kammenzind as well as the reprecipitation constant. The heat of transport, Q^* is 7 kcal/K, a value in the range proposed by Kammenzind and close to the Sawatzky' proposal. As the hydrogen migration ocurrs along the axial direction, the diffusivity in that direction is taken from Kearns. This choice produces the better fit to the measured data.

Figure 7 depicts the calculated and measured hydrogen profiles after the 25 days annealing. Also plotted are the calculated hydrogen concentrations in the α and δ phases at temperature as well as the corresponding TSS.

The agreement between the experimental and the calculated is rather good especially, the hydride dissolution front and general total hydrogen profile is well predicted.

The calculated profile changes slightly considering the TSS solvus determined by Une *et al.* as presented in Figure 8 but keeping the good fitting to the measured data. Also presented in this figure is the profile calculated ignoring the hysteresis effects. It makes clear that this is a key feature, ignored in most of the old and some of the more modern papers, to predict the hydrogen profile. If this feature is ignored, the hydrogen profile changes dramatically.

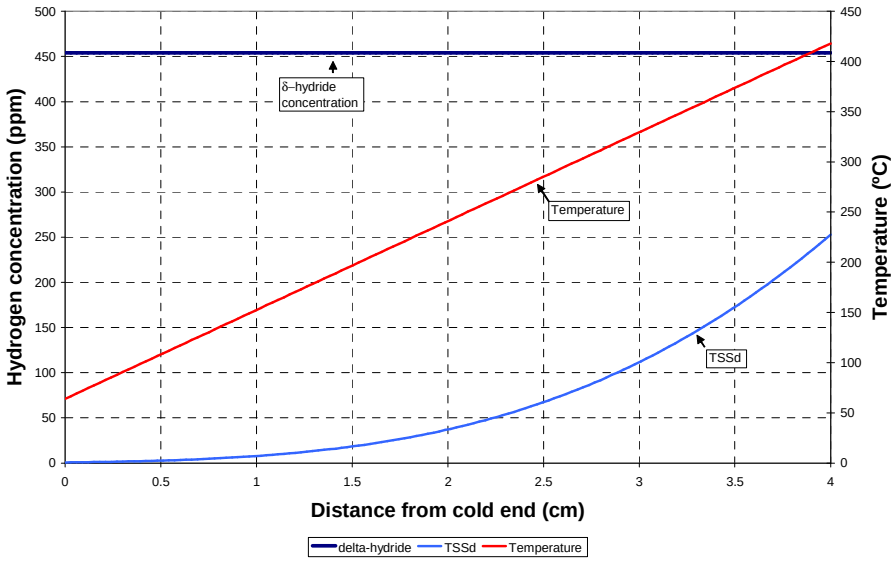

Figure 6: Temperature and hydrogen distribution at t_0 in Planman' specimen.

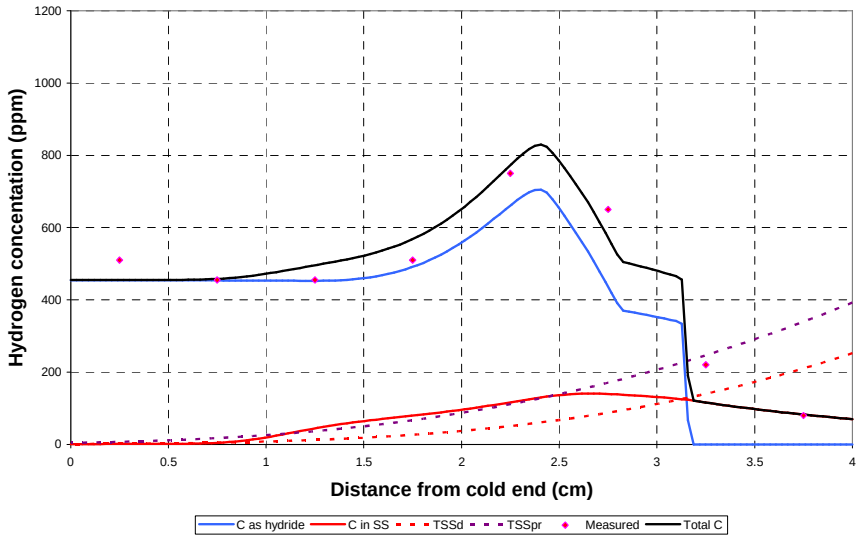

Figure 7: Measured and calculated hydrogen profiles after 25 days annealing in Planman's specimen.

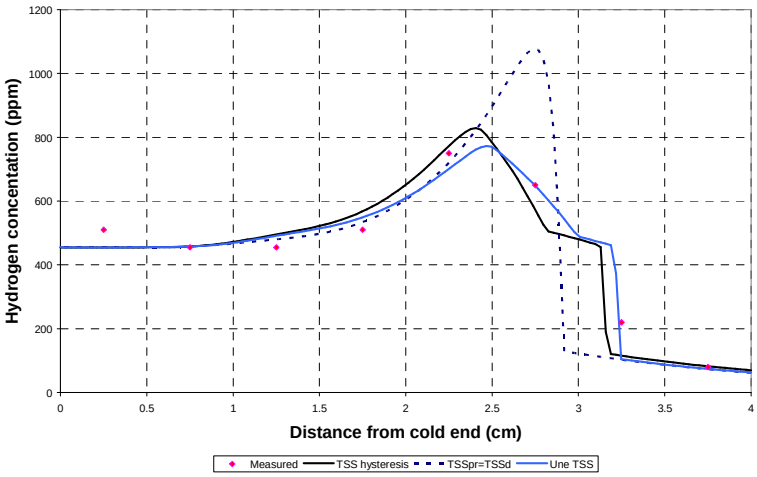

Figure 8: Effects of the TSS solvi and hysteresis in the calculated hydrogen profiles for the Planman' specimen.

Finally, it should be also pointed out that the position of the hydride dissolution front is also well predicted assuming that the hydride precipitation and dissolution rates are equal.

4.2 Sawatzky´s specimen

Sawatzky ran a test [40] used afterwards by many others to check their models adequacy. A thermal diffusion run in Zr-2 was made for a time duration too short, 34 days, to allow the hydrogen to reach a steady-state distribution. The specimen was 2.5 cm length, charged with an initial hydrogen concentration of 130 ppm. In this case, the colder and hotter end temperature was 130^o and 477 ^{o}C respectively *i.e.* the thermal gradient was 138 ^{o}C/cm.

Figure 9 depicts the inital hydrogen concentration and temperature distribution in this specimen as well as the TSS solvus accordding to Kammenzind's proposal. It should be noted that at the hotter end, the TSS_D is higher than the initial charged hydrogen therefore, the hydrogen in solid solution should be shortly after the heat-up to the annealing temperature, in solid solution. In this way, most of the hydrogen will be migrating to the colder end under the temperature gradient.

The specimen has been spatially discretized using 100 linear elements. The same material properties as for the Planman's specimen have been used: TSS_{PR} and TSS_D are taken from Kammenzind as well as the reprecipitation constant; the heat of transport, Q* is 7 kcal/K, and the diffusivity from Kearns.

Figure 10 depicts the measured hydrogen concentration as well as the calculated one after the 34 days annealing. The measured data was determined on

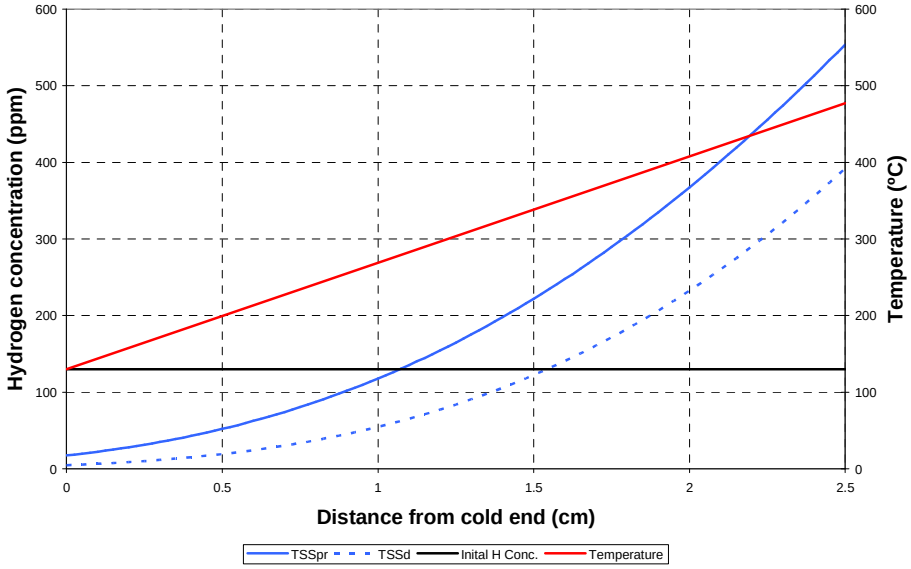

Figure 9: Hydrogen and temperature distribution in Sawatzky specimen

discs 0.1 cm thick by the hot-extraction method.

It is noted first that the highest measured hydrogen concentrations are well above the calculated values. However, the total hydrogen in the sample calculated from the measured profile is higher than the total precharged one thus, indicating a potential fault in these values. Whether this observation may be attributed to an oxide layer remaining in the sample at some positions, as reported for other specimens in the same paper, and contaminating the measured hydrogen or to other reasons, is unknown. This experiment is as far as the authors knowledge, the reported one using the largest temperature gradient thus, it is very valuable.

In this test case, there is a difference in the predictions obtained considering instantaneous and finite rate kinetics. In effect, at the colder end the instantaneous kinetics result in a hydride precipitation that acts as a sink of the migrating hydrogen. In this way, the total hydrogen content at the colder end increases devoiding the surrounding area from solid solution hydrogen and changing the hydrogen profile.

This very high concentrations in the colder ends are also observed in the Kamenzind *et al.*specimens [7] under a mild thermal gradients, 66^{o}C/cm and 7 ^{o}C/cm, but annealed at relatively high temperatures, 371 ^{o}C at the colder end. Accordding to the measured profile after the specimens annealing, it can be guessed that the initial hydrogen concentration was sufficiently low to be, basically, in solid solution. Unfortunately, some details, such as the initial hy-

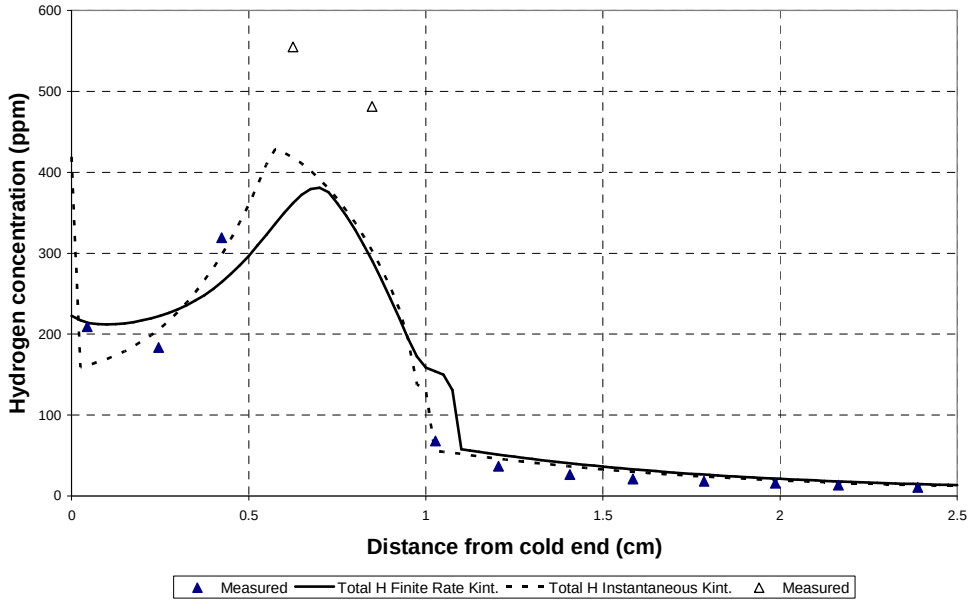

Figure 10: Measured and calculated hydrogen profiles in Sawatzky's specimen.

drogen content, are not given in Kammenzind paper so they cannot be modeled and these effects unequivocally verified.

4.3 Kammenzind diffusion couple

This test was designed by Kammenzind and coworkers [6] to check the impact of the precipitated hydride fraction in the terminal solid-solution solubility. The test results indicated that in the range of the tested hydrogen concentrations there were no discernible effects, and, as a side result, it also allowed to conclude by the authors that the hydride dissolution process was slower than the precipitation kinetics determined in a previous work [7]. Therefore, it will be used in this work for this latter purpose.

The specimen consisted of a diffusion couple from a Zr-4 plate in recrystallized condition, 2.54 cm length, one half precharged with 10 ppm and the other half with 435 ppm of hydrogen. The specimen was annealed during 100 days at 360°C and the resulting hydrogen profile measured using hot vacuum extraction on six samples of equal length. Figure 11 depicts the measured profile. It should be noted that the total hydrogen in the specimen after the annealing calculated from this profile is 6.4% higher than the initial one.

This specimen has been spatially discretized into 102 linear elements of equal length. The TSS solvi have been taken from Kammenzind as described in Section 2.3.1; in this case, the hydrogen concnetration in solid solution according to

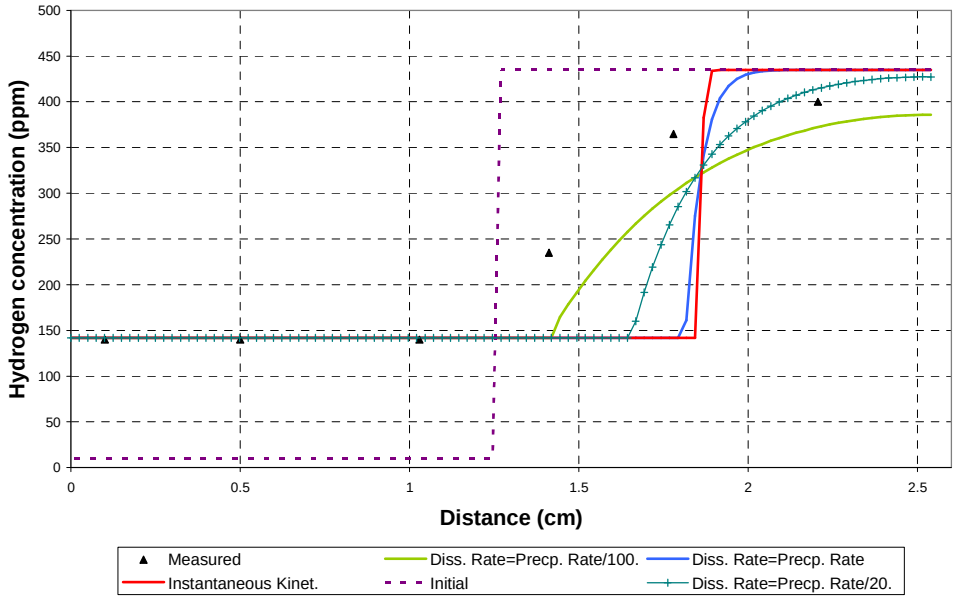

Figure 11: Hydrogen profiles in the Kammenzind diffusion couple after 100 days annealing.

the TSS_D is slightly higher, 152 ppm, than the measured one. Thus, the TSS_D has been slightly adjusted to predict exactly 140 ppm at the 360^oC annealing temperature. The diffusion coefficient has been taken from Kearns and the heat of transport is irrelevant in this case as there is no temperature gradient *i.e.* hydrogen migration is due to diffusion under a concentration gradient.

Figure 11 depicts the intial, measured and calculated hydrogen profiles under different assumption on the α^2 value for the dissolution process.

Either instantaneous and the assumption of $\alpha_{PR} = \alpha_D$ kinetics result in a dissolution front advancing from the low concentration to the high concentration end and very slow dissolution kinetics, $\alpha_D = \alpha_{PR}/10$, is needed to resemble the measured profile. Considering that the numerical method has preserved the total hydrogen in the sample, it is clear that the measured profile overstimate the total hydrogen in the sample, the reasons remaining unknown for the authors. However, these experimental results may indicate that hydride dissolution may be more sluggish than precipitation and that the proposed model is able to capture the experimental results if adequate material properties are available.

4.4 Formation of a hydride blister

This example checks the proposed model capabilities to solve multidimensional problems. The problem at hand is the formation of a hydride lens, also named

blister, in a Zr-alloy fuel rod cladding due to the partial lost of the waterside oxide layer formed during its irradiation in a light water nuclear reactor.

It has been observed that under some circumstances the thick oxide layer, of the order of 100 μm or larger, formed due to waterside corrosion during the fuel rod irradiation may be partially lost, spalled off, resulting in a cold spot in the fuel rod cladding. The hydrogen produced in the Zr-alloy corrosion reaction and already picked-up by the cladding, will migrate to this cold spot then, elevating the hydrogen content locally and eventually resulting in a pure $\delta-$hydride lens [32][5].

The cladding geometry considered in this example corresponds to a Pressurized Water Reactor 17x17 fuel rod with and outside diameter of 9.5 mm and thickness 0.57 mm. The fuel rod is assumed to be irradiated under a local heat flux of 70 W/cm^2 such as the cladding average content reaches 600 ppm under prototypical cladding temperatures, 375^{o}C at the cladding outer diameter. According to Garzarolli [11] a dense hydride rim will develop under these conditions. Fuketa *et al.* [45] obtained a hydride rim with thickness between 50 to 140 μm with hydrogen concentrations in the rim from 2000 to 3000 ppm when charging this type of cladding with up to 504 ppm, thickness average. Outside the rim, the hydrogen concentration in the Fuketa specimen ranges from 100 to 200 ppm.

Figure 12 depicts the 25^o cladding sector considered in the calculations along with the boundary conditions for the thermal problem. This cladding sector is spatially discretized using 2674 linear triangles from 1422 nodes.

Figure 13 presents the cladding temperature distribution calculated from the 70 W/cm^2 heat flux considering a Zr-alloy thermal conductivity

$$k = 9.37683 + 0.0118 \cdot T \ \ (W/mK)$$

taken from reference [18] and the resulting hydrogen distribution. It is observed that the hydrogen concentration at the cladding outside diameter is high, 6100 ppm, corresponding to a hydride fraction at room temperature of 36 %. This hydride rim extents along $\approx$60 μm. Outside the rim, the hydrogen concentration is low, of the order of 250 ppm. Therefore, this hydrogen profile agrees with the Fuketa reported profile.

Once this steady-state hydrogen distribution in the cladding thickness is achieved, a piece of the waterside oxide layer with azimuthal length of 2 mm ($\simeq$ 25^o apart) and located at $\theta = 0$, is assumed to spall off. The local lost of the oxide insulating layer, k=2.0 W/mK [18], results in a cold spot that changes the temperature distribution inside the cladding and produces, in turn, the hydrogen migration to the cold spot.

The oxide spalling-off is simulated by instantaneously reducing the temperature prescribed at the outside diameter to a lower value in the spalled area. This temperature reduction is calculated from the heat flux, 70 W/cm^2,the Zirconium oxide thermal conductivity, 2.0 W/mK, and assuming that only the pre-transition oxide remains, *i.e.* $\approx$80 μm from the initial 100 μm are lost. Then, the temperature reduction at the outer diameter of the cold spot site is

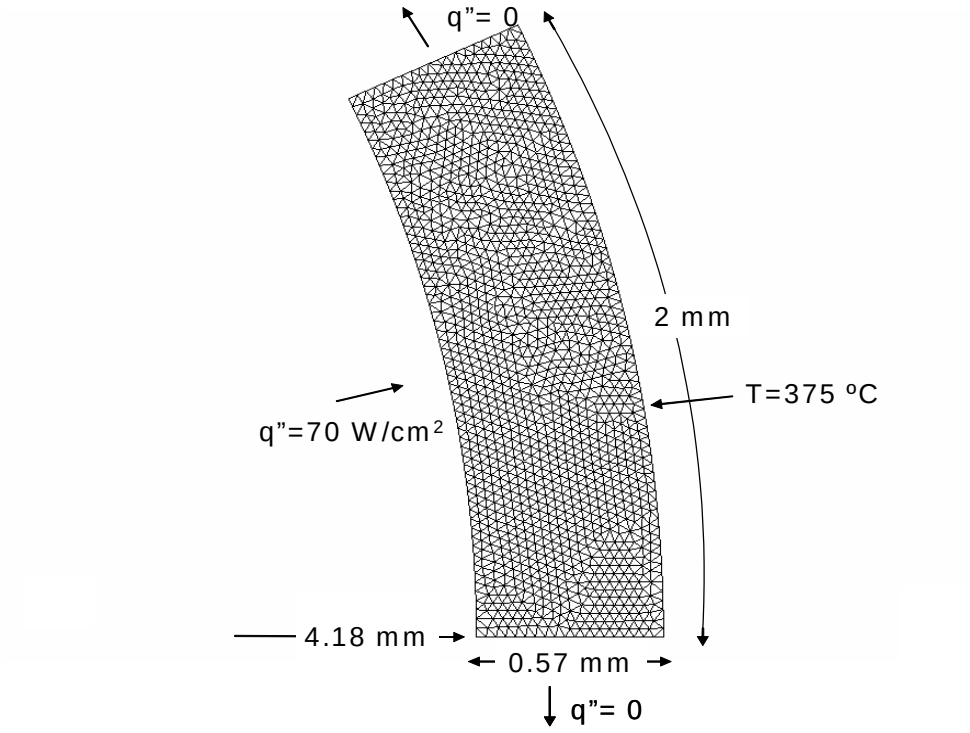

Figure 12: Domain considered in the blister formation calculations.

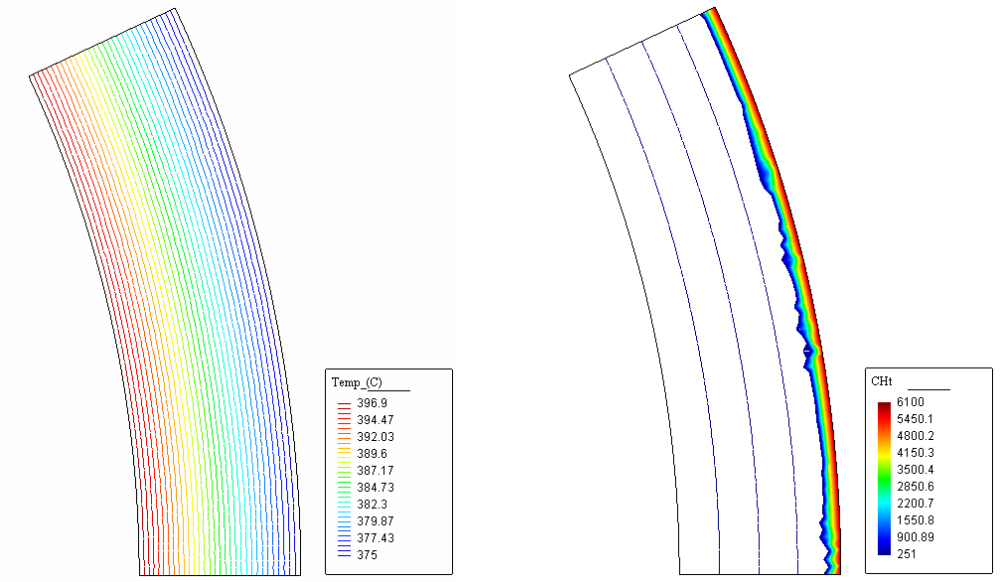

(a) Temperature distribution (b) Hydrogen concentration

Figure 13: (a) Temperature and (b) hydrogen distribution before oxide spalling off.

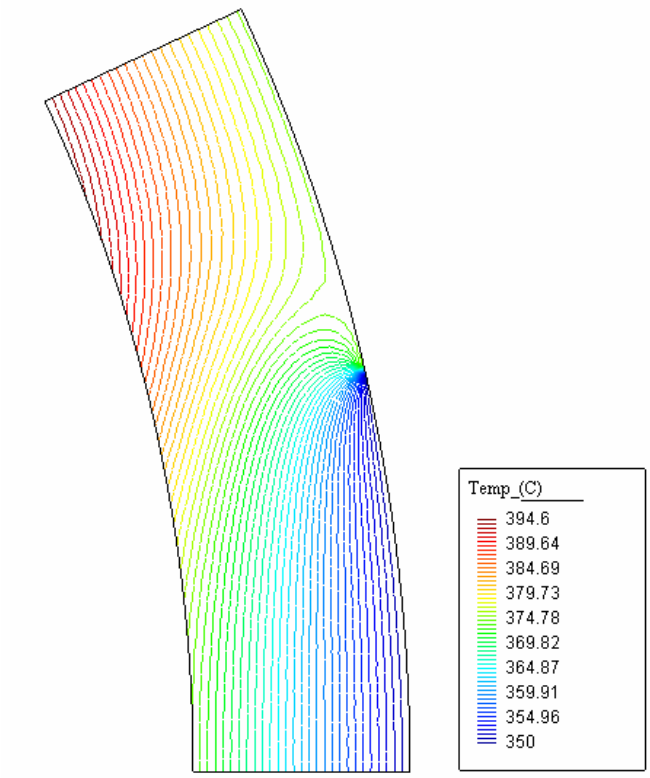

Figure 14: Temperature distribution in the cladding sector calculated assuming 25^oC reduction in the prescribed temeprature due to oxide spalling at $\theta = 0$.

$\approx 25^oC$. Figure 14 plots the temperature field calculated from these condtions assuming that the oxide spalling is centered at $\theta = 0$.

It should be noticed that the characteristic time, $t_c = (L/2)^2 D$ where L is the cladding thickness, of the heat conduction problem is much shorter, t_c=0.01s, than the corresponding to the hydrogen diffusion problem, t_c=350 s. Therefore, heat conduction operates in a much shorter time scale than the hydrogen diffusion and the transient heat conduction can not affect the hydrogen concentration profile. Thus, the change in the temperature field can be assumed as instantaneous.

This new temperature field modifies the hydrogen profile presented in Figure 13 as depicted in Figure 15. This latter figure depicts the contours of the steady-state hydrogen distribution calculated under this temperature field. It should be noticed that pure $\delta-$hydride now exists at the cladding outer diameter. This final shape is in overall well agreement with the hydrogen concentrations observed due to this oxide spalling phenomenon [5][32].

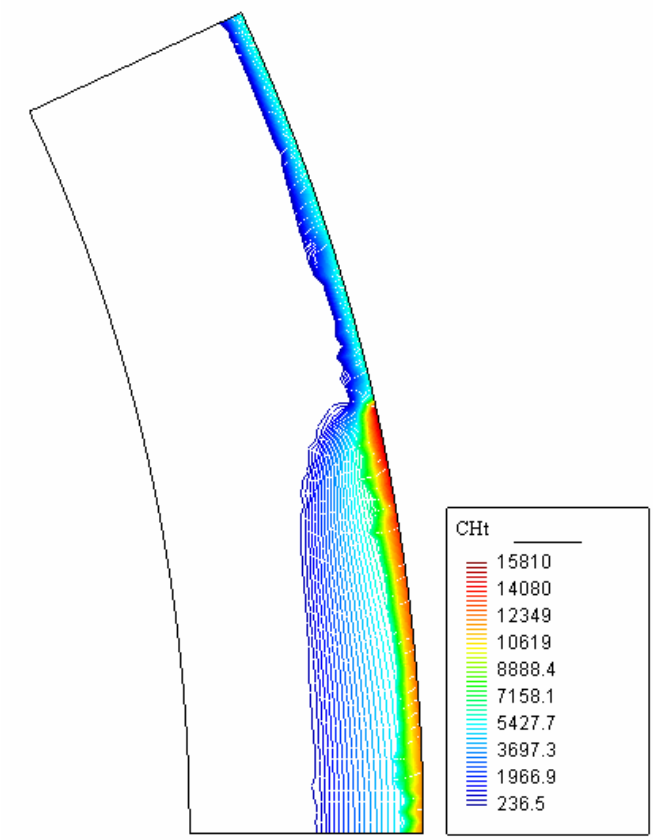

Figure 15: Effect of the temperature field after oxide spallation depicted inFigure 14, in the hydrogen distribution presented in Figure 13 (b).

5 Conclusions

A model for the thermally assisted diffusion of hydrogen in metals and its alloys, with special emphasys in the zirconium alloys used by the nuclear industry, has been presented. This model has been shown to be of advective-diffusive with sources type, the latter due to the metal-hydride precipitation/dissolution process that may occur. In this way, all the advances produced during the recent years in the field of the numerical solution of conservation equations can be used to solve the model equations.

The model equations are numerically solved using the Finite Element Method following an splitting procedure: first, the advection-diffusion equation ias solved using the well proved Two Step Taylor Galerkin and then, the ODE for the sources is integrated analytically. The solution of a number of experimental test cases supports the model adequacy to predict the hydrogen migration under a thermal gradient once the material properties are unknown. In these regards, the solution of the test cases indicates that consideration of the hysteresis effects and finite-rate kinetics are critical to predict the measured hydrogen profiles.

References

[1] A. McMinn, E.C. Darby and J.S. Schofield. The terminal solid solubility of hydrogen in zirconium alloys. In G.P. Sabol and G.D. Moan, editors, *Zirconium in the Nuclear Industry: Twelfth International Symposium, ASTM STP 1354*, pages 173–195. American Society for Testing and Materials, 2000.

[2] A. Sawatzky. The diffusion and solubility of hydrogen in the alpha-phase of Zircaloy-2. *J. Nuc. Materials*, 2(1):62–68, 1960.

[3] A. Sawatzky and E. Vogt. Mathematics of thermal diffusion of hydrogen in zircaloy-2. *Transactions of the metallurgical society of AIME*, 227:917, 1963.

[4] A.G. Varias and A.R. Massih. Hydride-induced embrittlement and fracture in metals-Effect of stress and temperature distribution. *Journal of the Mechanics and Physics of Solids*, 50:1469–1510, 2002.

[5] A.M. Garde, G.P. Smith and R.C. Pirek. Effects of hydride precipitate localization and neutron fluence on the ductility of irradiated Zircaloy-4. In E.R. Bradley and G.P. Sabol, editors, *Zirconium in the Nuclear Industry: Eleventh Symposium, ASTM STP 1295*, pages 407–428. American Society for Testing and Materials, 1996.

[6] B.F. Kammenzind, B.M. Berquist, R. Bajaj, P.H. Kreyns and D.G. Franklin. The long-range migration of hydrogen through zircaloy in response to tensile and compressive stress gradients. In G.P. Sabol and G.D. Moan, editors, *Zirconium in the Nuclear Indsutry: Twelfth International Symposium, ASTM STP 1354*, pages 196–233, 2000.

[7] B.F. Kammenzind, D.G. Franklin, H.R. Peters and W.J. Duffin. Hydrogen pickup and redistribution in alpha-annealed Zircaloy-4. In E.R. Bradley and G.P. Sabol, editor, *Zirconium in the Nuclear Indstry: Eleventh International Symposium, ASTM STP 1295*, pages 338–370, 1996.

[8] C.E. Coleman and D. Hardie. The hydrogen embrittlement of alpha zirconium- A review. *J. of Less-Common Metals*, 11:168–185, 1966.

[9] C.E. Ells and C.J. Simpson. Stress induced movement of hydrogen in zirconium alloys. In I.M. Bernstein and A.W. Thompson, editors, *International Conference on Hydrogen in Metals*, pages 345–360. AMS Metals Park, 1974.

[10] D.O. Northwood and U. Kosasih. Hydrides and delayed hydrogen cracking in zirconium and its alloys. *International Metal Reviews*, 28(2):92–120, 1983.

[11] F. Garzarolli, R. Manzel and A. Seibold. Corrosion phenomena in Zr-Alloy fuel claddings at high burnups. In *Tenth International Conference on Enviromental Degradation of Materials in Nuclear Power Systems-Water Reactors*, Lake Tahoe, 2001. NACE International.

[12] F. Schmitz and J. Papin. High burnup effects on fuel behaviour under accident conditions: The test CABRI REP-Na. *J. Nuc. Materials*, 270:55–64, 1999.

[13] G.C. Buscaglia and R.A. Enrique. Numerical solution of the thermally-assisted diffusion of hydrogen in zirconium alloys considering hysteresis and finite-rate kinetics. *Int. J. Num. Meth. Heat Fluid Flow*, 6(5):49–62, 1996.

[14] G.G. Libowitz. A pressure-composition-temperature study of the Zr-H system at high hydrogen contents. *J. Nuc. Materials*, 5:228–233, 1962.

[15] G.P. Marino. Hydrogen supercharging in Zircaloy. *Materials Science and Engineering*, 7:335–341, 1971.

[16] G.P. Marino. A numerical calculation of the redistribution of an interstitial solute in a thermal gradient. *Nuclear Science and Engineering*, 49:93–98, 1972.

[17] C. Hirsch. *Numerical Computation of Internal and External Flows*, volume 2. John Wiley & Sons, 1990.

[18] INEEL/EXT-02-00589. *MATPRO-A Library of Materials Properties for Light-Water-Reactor Accident Analysis*. Idaho National Engineering and Enviromental Laboratory, 2002.

[19] J. Lufrano, P. Sofronis and H.K. Birnbaum. Modelling of hydrogen transport and elastically accommodated hydride formation near a crack tip. *J. Mech. Phys. Solids*, 44(2):179–205, 1996.

[20] J.B. Bai, C. Prioul, S. Lansiart and D. Francois. Brittle fracture induced by hydrides in Zircaloy-4. *Scripta Metallurgica etr Materialia*, 25:2559–2563, 1991.

[21] J.C.M. Li, R.A. Oriani and L.S. Darken. The thermodynamics of stressed solids. *Zeitschrift für Physikalische Chemie Neue Folge*, 49:271–290, 1966.

[22] J.M. Markowitz. The thermal diffusion of hydrogen in alpha-delta Zircaloy-2. *Transactions of the Metallurgical Society of AIME*, 221:819–824, 1961.

[23] K. Une and S. Ishimoto. Dissolution and precipitation behavior of hydrides in Zircaloy-2 and high Fe Zircaloy. *J. Nuc. Materials*, 322:66–72, 2003.

[24] R. A. L.A. Simpson. Mechanics of hydrogen induced delayed cracking in hydride forming materials. *Metallurgical Transactions A*, 8A:1553–1562, 1977.

[25] J. Lemaitre and J.-L. Chaboche. *Mechanics of Solid Materials*. Cambridge University Press, 1990.

[26] M. Quecedo, M. Pastor, M.I. Herreros and J.A. Fernández Merodo. Numerical modelling of the propagation of fast landslides using the finite element method. *Int. J. for Num. Met. Eng.*, 59:755–794, 2004.

[27] G. Marino. HYDIZ-a 2-dimensional computer program for migration of interstitial solutes of finite solubility in a thermal gradient. *WAPD-TM-1157*, 1974.

[28] M.P. Puls. Elastic and plastic accomodation effects on metal-hydride solubility. *Acta metall.*, 32(8):1259–1269, 1984.

[29] O.C. Zienkiewicz and R.L. Taylor. *The Finite Element Method*, volume 2. McGraw-Hill, fourth edition, 1991.

[30] Olivier O. Courty, Arthur T. Motta and Jason D. Hales. Modeling and simulation of hydrogen behavior in zircaloy-4 cladding. *J. Nucl. Mater.*, 452:311–320, September 2014.

[31] P. Efsing. *Delayed Hydride Cracking in Irradiated Zircaloy*. PhD thesis, Royal Institute of Technology, Stockholm, Sweden, 1998.

[32] P. Guedeney, M. Trotabas, M. Boschiero, C. Forat and P. Blanpain. FRAGEMA fuel rod behaviour characterization at high burnup. In *ANS Topical Meeting on LWR Fuel Performance*, pages 627–638, Avignon, 1991. ANS/ENS.

[33] P. Shewmon . *Trans. AIME*, 233:736, 1965.

[34] P. Shewmon. *Diffusion in Solids*. The Minerals, Metals & Materials Society, second edition, 1989.

[35] P. Sofronis and J. Lufrano. Interaction of local elastoplasticity with hydrogen: Embrittlement effects. *Materials Science and Engineering*, (A260):41–47, 1999.

[36] J. Peraire. *A Finite Element Method for Convection Dominated Flows*. PhD thesis, University of Wales, Swansea, 1986.

[37] P.M. Gresho and R.L. Sani. *Incompressible Flow and the Finite Element Method*, volume 1. Advection-Diffusion. John Wiley & Sons Ltd., 1998.

[38] R.L. Kesterson, S.J. King and R.J. Comstock. Impact of hydrogen on dimensional stability of fuel assemblies. In *Proceedings, ANS Light Water Reactor Fuel Performance Conference, Park City, Utah*, Park City, Utah (USA), 2000.

[39] R.L.Eadie, K. Tashiro, D. Harrington and M. Leger. The determination of the partial molar volume of hydrogen in zirconium in a simple stress gradient using comparative microcalorimetry. *Scripta Metallurgical*, 26:231–236, 1992.

[40] A. Sawatzky. Hydrogen in Zircaloy-2: Its distribution and heat of transport. *J. of Nuc. Materials*, 2(4):321–328, 1960.

[41] S.R. de Groot and P. Mazur. *Non-Equilibrium Thermodynamics*. North-Holland Publishing Company, 1962.

[42] S.R. MacEwen, C.E. Coleman, C.E. Ells and J.Faber Jr. Dilation of hcp zirconium by interstitial deuterium. *Acta metall.*, 33:753–757, 1985.

[43] S. Suresh. *Fatigue of Materials*. Solid State Science Series. Cambridge University Press, first edition, 1991.

[44] T. B. Massalski, J. L. Murray, L. H. Bennett and H. Baker, editors. *Binary Alloy Phase Diagrams*. Second edition, 1986.

[45] T. Fuketa, T. Nakamura, H. Sasajima, F. Nagase, H. Uetsuka, K. Kikichi and T. Abe. Behaviour of PWR and BWR fuels during reactivity initiated accident conditions. In *Proceedings ANS Light Water Reactor Fuel Performance Conference, Park City, Utah*, 2000.

[46] T. Kido, K. Kanasugi, M. Sugano and K. Komatsu. PWR zircaloy cladding corrosion behaviour: Quantitative analyses. *J. Nuc. Materials*, 248:281–287, 1997.

[47] T. Planman and J. Freund. *Thermal Diffusion of Hydrogen in Zirconium Alloys*. VTT-MET B-237, 1993.

[48] T.B. Flanagan, N.B. Manson and H.K. Birnbaum. *Scripta Metall.*, 15:109–112, 1981.

[49] E. Toro. *Riemann Solvers and Numerical Methods for Fluid Dynamics. A Practical Introduction.* Springer-Verlag, Berlin, 2nd edition, 1999.

[50] E. Toro. *Shock-Capturing Methods for Free-Surface Shallow Flows.* John Wiley & Sons, 2001.

[51] O. Zienkiewicz and R. Taylor. *The Finite Element Method, Fifth Edition.* Butterworth-Heinemann, 2000.

[52] Z.L. Pan, I.G. Ritchie and M.P. Puls. The terminal solid solubility of hydrogen and deuterium in Zr-2.5Nb Alloys. *J. Nuc. Materials*, 228:227–237, 1996.